Received July 31, 2020, accepted August 25, 2020, date of publication August 31, 2020, date of current version September 14, 2020.

Digital Object Identifier 10.1109/ACCESS.2020.3020403

Constellation Design for Single Photodetector Based CSK With Probabilistic Shaping and White Color Balance

DIL NASHIN ANWAR, (Graduate Student Member, IEEE), AND ANAND SRIVASTAVA, (Member, IEEE)

Department of Electronics and Communication, Indraprastha Institute of Information Technology Delhi (IIIT-D), New Delhi 110020, India

Corresponding author: Dil Nashin Anwar (dilnashina@iiitd.ac.in)

ABSTRACT Research and development of Li-Fi (Light Fidelity) in Internet-of-things (IoT) has created significant interest among researchers. The low-cost version of standard color shift keying (CSK) modulation scheme having single photodetector (PD) at the receiver can become an alternative to on-off keying (OOK) in IoT sensor networks as an M-ary CSK modulation scheme provides log_2M times more data rate than that of OOK. This work revolves around optimizing the constellation points of single PD based CSK (CSK-1PD) to achieve a more power-efficient modulation scheme. The optimization has been done with and without average white tone constraint for uniform and non-uniform (exponential, Maxwell-Boltzmann, Pareto) source distributions. The constellation design strategy is based on maximizing the minimum distance among the differently distributed symbols. In the case of non-uniform distributions, the constellations points have been optimized by geometrically shaping the points based on their probabilistic shaping (PS). The optimized constellation points (OCPs) of CSK-1PD without white tone constraint provide higher signal-to-noise ratio (SNR) gain at forward error correction (FEC) limit symbol error rate (SER) as compared with strict white tone constraint. Further, the strict white tone constraint has been relaxed by considering the whole white light region in the CIE 1931 chromaticity diagram as white tone. The OCPs for uniform data with relaxed white tone constraint achieves SNR gain similar to without white tone constraint. However, for probabilistically shaped symbols, the SNR gain achieved from OCPs improves from strict white tone constraint but remains less than the without white tone constraint. A novel method to utilize an additional RGB LED at the transmitter side has been proposed and designed to maintain any white tone light in the white light region without degrading the maximum achieved SNR gain.

INDEX TERMS Colour shift keying (CSK), constellation optimization, probabilistic shaping (PS), visible light communication (VLC).

I. INTRODUCTION

The exponentially increasing demand for wireless data with the onset of wireless devices and internet of things (IoT) everywhere has created scarcity in the radio frequency (RF) spectrum. The existing overcrowded RF spectrum has impelled the hunt for newer technologies. Visible light communication (VLC), having a large amount of unlicensed spectrum, is an emergent alternative technology to supplement the existing short-range wireless systems for faster data transmissions. VLC has numerous unrivalled potentials along with immunity to every day electromagnetic interference, for instance, low energy consumption, data confinement for higher-level security and cheaper installation with existing illumination infrastructure [1]–[3].

The less computationally complex modulation schemes for VLC include on-off-keying (OOK), pulse position modulation (PPM), and colour intensity modulation (CIM). However, as per IEEE 802.15.7 standard [4] for VLC, these modulation schemes can cause large inrush currents when used with large arrays of LEDs and require constant flicker management [5]. The power controlled version of CIM, known as colour shift keying (CSK) can be an alternative. The optical power of the visible light emitted by multi-colour LEDs such as red, green and blue (RGB) LEDs in the tri-chromatic LED (TLED) lighting source is modulated for data transmission keeping constant signal envelope power. The RGB LEDs in CSK modulates data to provide

The associate editor coordinating the review of this manuscript and approving it for publication was Miguel López-Benítez.

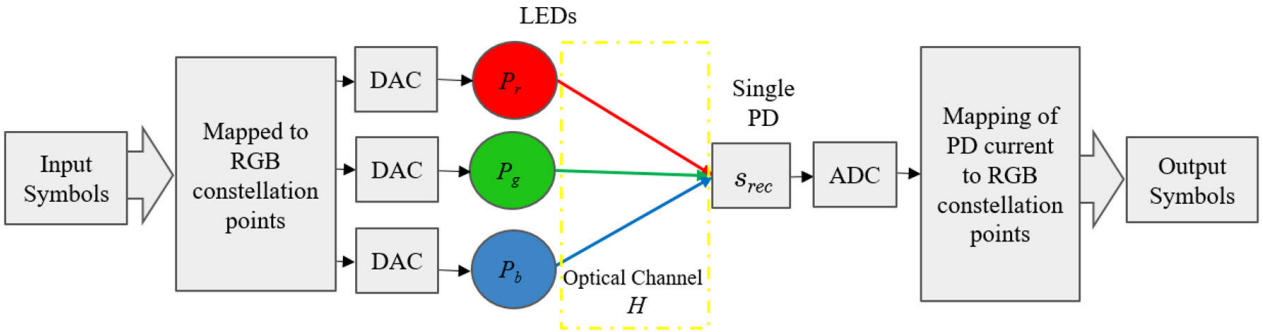

FIGURE 1. Block diagram of CSK-1PD (single photodetector based CSK) system.

communication along with illumination for indoor environments in buildings. CSK maintains a constant instantaneous luminance across each constellation, preventing intensity flicker and sudden flux of currents in LED devices. Thus, CSK reduces the imminent human health complications, such as nausea and epilepsy, related to light intensity fluctuations [5], [6]. The proposed work optimizes constellation points for single photodetector based CSK (referred to as CSK-1PD).

A. BACKGROUND: CSK-1PD

Fig.1 shows the block diagram of single photodetector based CSK (CSK-1PD) modulation scheme in VLC [7]. CSK-1PD utilizes the property of photodetector (PD) to generate specific electrical current to an incident optical power of a given wavelength. The electrical current s generated at the PD is linearly related to the transmitted optical LED power and the PD responsivity $\boldsymbol{\rho}$ at each red, green and blue wavelength of the RGB LED as shown in (1). The optical power of red, green, and blue LED lights are denoted by P_r, P_g, and P_b, respectively.

$$s = \langle \boldsymbol{\rho} \cdot \mathbf{p} \rangle. \tag{1}$$

The arithmetic operator $\langle \cdot \rangle$ in (1) defines the inner product between the transmitted RGB optical power vector, $\mathbf{p} = [P_r, P_g, P_b]^T$ such that $P_r + P_g + P_b = P_T$, satisfying the constant output power criteria. The PD responsivity vector, $\boldsymbol{\rho} = [\rho(red), \rho(green), \rho(blue)]$ where, the vector $\boldsymbol{\rho} = [0.42, 0.32, 0.22]$ has been obtained from the response curve of a practical PD (PDA36A2) from Thorlabs [8] for the central wavelength of red (640 nm), green (530 nm) and blue (465 nm) light respectively. PDA36A2 detects light signals ranging from 350 to 1100 nm and comes with an inbuilt gain amplifier. The power received at the PD is affected by the channel gain (H) and noise w. The proposed work considers the most accepted and widely used indoor VLC channel gain, i.e., DC optical channel gain with additive white Gaussian noise (AWGN) at the receiver PD [9], [10]. The received electrical current s_{rec} at the output of the PD is represented through equation (2).

$$s_{rec} = sH + w. \tag{2}$$

The constellation symbols of M-CSK-1PD at the transmitter side can be represented by RGB optical powers whereas at the receiver side it is physically realized with electrical currents and denoted by symbols ($s_i, i \in 1, 2, \ldots M$). M is the number of different symbols. The receiver performs symbol detection in M-CSK-1PD by computing the minimum Euclidean distances between the received and the transmitted symbols in the form of electric currents.

One of the primary criteria of any VLC modulation schemes is to maintain illumination with white tonality. The average color obtained from the CSK constellation symbols may not always lie inside the white region of the CIE 1931 chromaticity diagram, which generates color unbalances perceived by the human eye [7], [11]. IEEE 802.15.7 standard has already proposed the adoption of a pseudo-random sequence, known as scrambler to overcome the color unbalance problem. The scrambler has been used at the transmitter in [7] to maintain an average white tone output light in CSK-1PD for uniform input data. The actual input data can be obtained at the receiver by a descrambler.

B. RELATED WORK

The growing interests on designing and optimizing the constellation points mostly in terms of reduced received bit/symbol error rate for standard CSK over the past few years have led to the emergence of diverse techniques in the literature. Most of the constellation design problems aim to improve color balancing limitations or data rate transmissions. The authors in [11] proposed a genetic algorithm to design the constellation symbols for multiple LED transmitters at different wavelengths in the VLC system. Drost and Sadler are the first ones to investigate billiards algorithms for the design of CSK constellation points in [12]. Later, in paper [13], they compensated the channel distortions by designing a framework for optimizing the constellation points for VLC systems employing multiple emitters at different wavelengths. In [14], Monteiro *et al.* designed constellation points for CSK using interior-point methods and extended it to higher-order CSK constellations in [5]. In [15], the authors presented a power-efficient high dimensional constellation design scheme for the standardized TLEDs. To the best of

the authors' knowledge, the constellation design of CSK-1PD has been performed solely in [7] till date, which has stated numerical optimization solution for designing CSK-1PD constellations points for uniform input data.

C. MOTIVATION AND PROPOSED WORK

CSK-1PD is a low-cost color space-based modulation scheme [7], which can be exploited in Li-Fi (light fidelity) in IoT indoor scenario. CSK-1PD modulation scheme can be utilized in implementing IoT sensor networks in a smart home or hall scenario for communication as well as illumination, where resources are constrained and thus, low-cost and power-efficient systems are preferred. CSK-1PD constellations can be designed for maximum power efficiency in terms of low signal-to-noise ratio (SNR) required at forward error correction (FEC) limit symbol error rate (SER) within its optimization constraints.

Limited research work has motivated the authors to design optimized constellation points for CSK-1PD modulation scheme. The proposed work consists of designing optimized constellation points for CSK-1PD with uniform input data and then with three different non-uniform probabilistically shaped (exponential, Maxwell-Boltzmann, and Pareto) input data. Additionally, CSK-1PD with the four different input data types are optimized considering white color balance. Finally, a novel method to maintain any desired white tone light as CSK-1PD modulated output light has been proposed.

D. CONTRIBUTION

The key contribution of the proposed work can be enumerated as follows:

1) This article proposes a rigorous framework to design and optimize the constellation points for uniform and non-uniform source distribution in CSK-1PD to reduce the received SER.
2) The constellation points of non-uniformly distributed input symbols in CSK-1PD are optimized by geometrically shaping (GS) the symbols based on their preceding probabilistic shaping (PS). The consecutive PS-GS technique to optimize the constellation points has been scantly investigated hitherto.
3) A relaxed white tone constraint has been formulated by considering the whole white light region in CIE 1931 chromaticity diagram to maintain a white color balance with reduced SER.
4) A novel technique to maintain any desired average white tonality light without degrading the SNR gain by inserting an extra RGB LED at the transmitter.

The remainder of this article is structured as follows; Section II introduces the constellation optimization problem and proposes the objective functions. Section III mentions the constraints of the optimization problem statements with different aspects. The novel solutions to maintain average white tone have been proposed in Section IV. Section V analyzes and discusses the results. Finally, Section VI presents the conclusions.

Notations: The vector and the matrix are denoted as $\mathbf{x}$ and $\mathbf{X}$ respectively. The rows of matrix $\mathbf{X}$ is denoted as $\mathbf{X_R}$. The objective function for optimization is denoted by $\mathcal{F}(\mathbf{X})$. The set of pairwise Euclidean distance is denoted by d_k. The average of a scalar is denoted by $\bar{x}$.

II. CONSTELLATION DESIGN AND OPTIMIZATION

A. PROBLEM FORMULATION

In this article, the constellation optimization problem is formulated by adopting the widely accepted constellation design problem. It defines a constrained optimization strategy that maximizes the minimum Euclidean distance among the constellation symbols ($s_{i,j}$) while maintaining some of the aspects such as constant output power, average white color balance with and without PS. The constellation points are designed for the minimization of SER at the receiver. The optimization problem, as shown in (3), becomes a max-min problem, and therefore the objective function becomes a non-convex problem [16]. The pairwise Euclidean distance of symbols s_i and s_j is denoted by $|s_i - s_j|$. The objective function is both non-convex and non-differentiable, making it difficult to solve analytically [7], [14]. Further, the minimum function of the objective function is discontinuous, which makes it incompatible with efficient, gradient-based techniques [11]–[14]. The $M = 4$ constellation symbols ($s_{i,j}$) have been investigated in the paper for CSK-1PD which are in the form of electrical currents.

$$\begin{aligned} &\text{maximize} \quad \min_{\substack{i,j\in\{1,\ldots,M\} \\ i\neq j}} |s_i - s_j| \\ &\text{subject to} \quad \textit{constraints} \text{ (described in section III).} \end{aligned} \tag{3}$$

B. OBJECTIVE FUNCTION

To solve this non-convex problem, researchers have suggested many approaches; one of them is the differential approximation which removes the non-differentiable nature by using well known ''log sum-exponentials'' continuous approximation [16]. The approximated objective function in (4) still remains non-convex; however, optimization techniques based on the derivation of the Hessian of the objective function can find the locally optimal symbol sets. For non-convex problems, commercially available optimization algorithms exclusively discover local minima [14]. However, the likelihood of realizing a global optimum is improved by optimizing the objective function multiple times over a small set of random starting points and tuning the β parameter where β determines the accuracy of the approximation between (3) and (4) as discussed in [11].

The PS of input data already provides SNR gain in optical fiber and VLC systems [17]–[19]. The optimized constellation points obtained from (4) for uniform input data can be further optimized for non-uniform input data by adapting the concept of hybrid probabilistic shaping and geometric shaping [18], [21]. The PS CSK-1PD constellation points

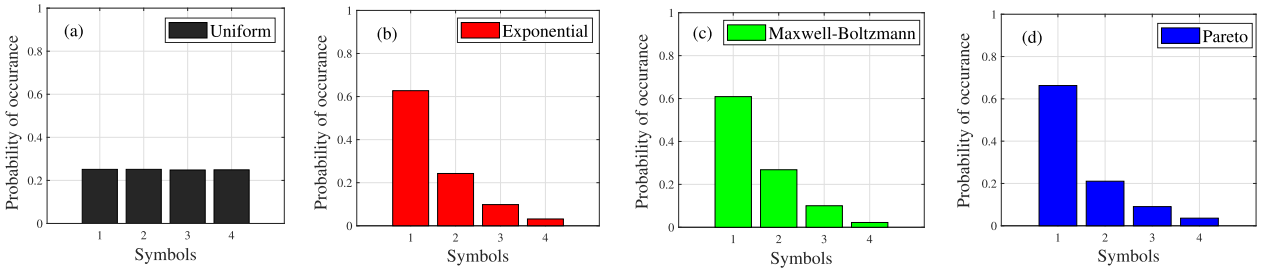

FIGURE 2. PDF of (a) uniform, (b) exponential, (c) Maxwell-Boltzmann and (d) Pareto source distributions for 4-CSK-1PD scheme.

are designed in the confined region of constellation symbols according to the probability of occurrence of symbols. Therefore, the PS constellation symbols are shifted geometrically according to the known PS of the symbols to get minimum SER. Hence, the objective function in (4) needs to be modified to include the probability of symbols.

$$\begin{aligned} &\text{maximize} \quad -\frac{1}{\beta}\ln\left(\sum_{\substack{i,j\in\{1,\ldots,M\}\\ i\neq j}} e^{-\beta|s_i-s_j|}\right) \\ &\text{subject to} \quad \textit{constraints} \text{ (described in section III).} \end{aligned} \tag{4}$$

$$\begin{aligned} &\text{maximize} \quad -\frac{1}{\beta}\ln\left(\sum_{\substack{i,j\in\{1,\ldots,M\}\\ i\neq j\\ p(s_i)>p(s_j)}} e^{-\beta|s_i-s_j|\ln\frac{p(s_j)}{p(s_i)}}\right) \\ &\text{subject to} \quad \textit{constraints} \text{ in section III.} \end{aligned} \tag{5}$$

The PS in constellation symbols follows optimum probability order obtained in [19], employing the highest probabilities to the minimum error causing pair of symbols. The probability of occurrence of symbols $p(s)$ for non-uniform source distributions has been calculated at unity achievable information rate (AIR) to match it with the uniform source distribution AIR, to retain a consistent AIR in results for a fair comparison [19]. The plot of probability distribution function (PDF) of 4-CSK-1PD for uniform, exponential, Maxwell-Boltzmann, and Pareto source distributions at unity AIR has been presented in Figs. 2 (a), 2 (b), 2 (c), and 2 (d), respectively. The optimum probability order for CSK-1PD in an AWGN channel follows $p(s_1) > p(s_2) > p(s_3) > p(s_4)$ where $s_1 < s_2 < s_3 < s_4$.

When the symbols are non-equiprobable the detection threshold for received signal in an AWGN channel shift from the midway point between two symbols based on the logarithmic ratio of the probability of occurrence of symbols [20]. Henceforth, the pairwise Euclidean distances of non-equiprobable symbols get affected by the logarithmic ratio of the likelihood of occurrence of symbols as shown in (5). The logarithmic ratio alters the pairwise Euclidean distances so that the minimum of log sum-exponentials procures the pairwise Euclidean distance of minimum error causing pair of symbols.

C. OPTIMIZATION ALGORITHM

As stated in section II. *B*, finding the analytical solution of the non-convex optimization problem becomes a difficult task, so usually, this type of optimization problem is solved with numerical optimization algorithms [22]. The continuous approximated objective functions can be solved using commercially available algorithms such as MATLAB's *fmincon*, which finds the minimum of a constrained nonlinear multivariable function. The maximum of a function can also be found by *fmincon*, by taking negative of the functions in (4) and (5). This work utilizes MATLAB's *fmincon* based on an interior-point algorithm to obtain the optimized constellation points (OCPs) of CSK-1PD with the constraints (explained in the upcoming section III). The numerical optimization algorithm process is summarized in Algorithm 1. The objective function $\mathcal{F}(\mathbf{X})$, has been formulated for constellation points in the form of matrix $\mathbf{X}$. The set of pairwise Euclidean distances is denoted by (6), which can be obtained from matrix $\mathbf{X}$ and a sparse matrix formed out of $\boldsymbol{\rho}$.

$$d_k = \{|s_i - s_j|\} \quad \forall \begin{cases} i,j \in \{1,\ldots,M\}, \\ i \neq j \\ k \in \{1,\ldots,\binom{M}{2}\}. \end{cases} \tag{6}$$

The tuning parameter β in Algorithm 1 produces poor result for smaller values, whereas, for arbitrarily large values, the large gradients cause the algorithm to converge slowly. Therefore, the objective function applies the interior point method for multiple iterations, starting with a smaller β and increasing β in each iteration [14]. This approach provides a reliable approximation without slow convergence and with each successive β the optimal solution of the previous β acts as the starting point for the next. However, the solution obtained at each successive β may not always be feasible with respect to the linear inequality constraints. Therefore, in Algorithm 1, the basic concept of the genetic algorithm to produce good solutions by avoiding the trajectory towards bad solutions has been used [23]. It helps in avoiding the non-feasible solutions. The minimum Euclidean distance (MED) constraint updates itself for every feasible solution and thus along with genetic algorithm reduces the number of iterations for the optimization process with β. The SER of feasible solutions at design SNR is calculated until

the occurrence of the first non-feasible solution to form a potential population set P_{SNR}. The choice of design SNR is medium to high SNRs as the SER expression with union upper bound is fairly tight in those SNRs [24]. Further, the SER is greater than 0.5 in SNRs below 15 dB, optimizing points for lower SNRs may not completely optimize the points for higher SNRs. This work is looking for SNR gain at FEC limit SER. Hence, the design SNR is 15 dB, the average of SNRs at worst, and FEC limit SER. For faster computation the theoretical CSK-1PD SER expression from [19] has been considered in the algorithm, as shown in (7).

$$P_e = \sum_{i=1}^{M-1}\left[\frac{p(s_i)}{2}\text{erfc}\left(\sqrt{\frac{(d_i^2+\Gamma_i)^2}{4d_i^2N_0}}\right) + \ldots\frac{p(s_{i+1})}{2}\text{erfc}\left(\sqrt{\frac{(d_i^2-\Gamma_i)^2}{4d_i^2N_0}}\right)\right], \quad (7)$$

where,

$$d_i = |s_i - s_{i+1}| \quad \forall \left\{i \in \{1,\ldots,M-1\},\right.$$
$$\Gamma_i = N_0 \ln\frac{p(s_i)}{p(s_{i+1})} \quad s.t.\ p(s_i) \geq p(s_{i+1}). \quad (8)$$

The apriori probability of symbol s_i is represented by $p(s_i)$ and N_0 is the noise variance. At the occurrence of non-feasible solution the best fitting solution, i.e., the constellation points providing minimum SNR from the potential population set is chosen as the starting point. The solutions obtained by the numeric algorithm depend on the initial estimate of the constellation points (**X0**) used to start the optimization process [21]. The random starting points must be a strictly feasible constellation points (as shown in Table. 1), fulfilling the optical power and geometric constraint with strict inequality range constraint (as explained in section III). The constellation symbols are represented by s_i, where $i = \{1, 2, 3, \ldots M\}$. Algorithm 1 can be used for optimizing constellations of any size with arbitrary convex constraints.

Algorithm 1 Numerical Optimization Algorithm

Initialize: Random initial constellation points, **X0**, satisfies power, geometric and range constraints.
$\mathbf{X} \leftarrow \mathbf{X0}$
$\beta \leftarrow 1$
for $\beta \leq$ 1000 **do**
  $\mathcal{F}(\mathbf{X}) \leftarrow \max \quad -\frac{1}{\beta}\ln\left(\sum_{k=1}^{\binom{M}{2}} e^{-\beta d_k}\right)$
  subject to Constraints.
  if X obtained satisfies the constraints to become a feasible solution **then**
    $\mathbf{X0} \leftarrow \mathbf{X}$
    $\{P_{SNR}\} \leftarrow \text{SNR}(\mathbf{X})$
    MED Constraint(**X0**) $\leftarrow$ MED Constraint(**X**)
    $\beta \leftarrow \beta + 2$
  end
  else
    non-feasible solution obtained
    $\mathbf{X0} \leftarrow \mathbf{X}$, where **X** provides min $\{P_{SNR}\}$
  end
end
return ($\mathbf{X}_o$)

III. CONSTRAINTS FORMULATION

The constellation design in CSK-1PD scheme for uniform input data without white color balance requires optical power based constraint, geometric and range constraint. Additionally, it requires MED constraint, which updates with updated starting constellation points **X0** in the optimization process in Algorithm 1. For non-uniform input data; optical power, geometric and range constraints remain the same, whereas the PS of symbols modifies the MED constraint as shown in section III-C. Later, to maintain white-tone output light in both uniform and non-uniform source distributions, color constraints have been discussed.

A. OPTICAL POWER CONSTRAINT

The signal envelope in CSK scheme has a non-varying power as it modulates data for constant output power. Constellation points have been designed to keep the desired total optical power, P_T, as a positive non-zero constant. The optical powers P_r, P_g, and P_b may take any non-negative value less than its peak values (9). P_{pr}, P_{pg}, and P_{pb} denote the peak optical powers of red, green, and blue LEDs, respectively. The peak powers and P_T are considered 1 to work on normalized values. The constant optical power constraint is analogous to the constant energy condition of many optimization processes. The optical power constraint, as shown in (10) is a mandatory constraint for designing constellation points in CSK-1PD.

$$0 \leq P_r \leq P_{pr},$$
$$0 \leq P_g \leq P_{pg},$$
$$0 \leq P_b \leq P_{pb}. \quad (9)$$
$$P_r + P_g + P_b = P_T. \quad (10)$$

TABLE 1. Random 4-CSK-1PD Constellation Points. The light-grey shaded part forms the matrix **X0**.

RGB optical power vector	P_r	P_g	P_b	Symbols in normalized current
$\mathbf{p}_1$	0	0	1	$s_1 \rightarrow 0.220$
$\mathbf{p}_2$	0.2503	0.2884	0.4612	$s_2 \rightarrow 0.299$
$\mathbf{p}_3$	0.4732	0.2799	0.2469	$s_3 \rightarrow 0.340$
$\mathbf{p}_4$	1	0	0	$s_4 \rightarrow 0.420$

B. GEOMETRIC AND RANGE CONSTRAINT

The geometric condition for CSK-1PD symbols as shown in (11) is that each vector formed by the difference of any two symbols should not be orthogonal to the responsivity vector $\boldsymbol{\rho}$ (as discussed in section I-A). It is simply to avoid same electric current s at the receiver, from any of the two constellation points so as to have a distinct set of

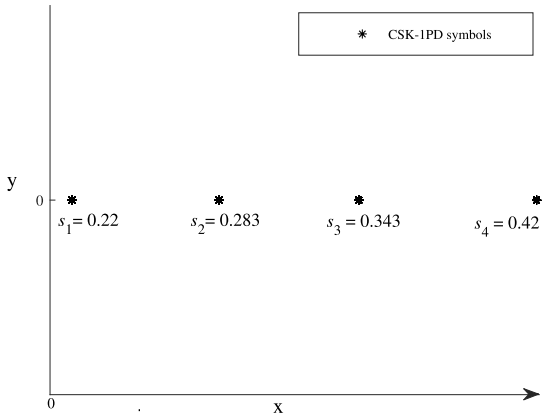

FIGURE 3. Constellation diagram of CSK-1PD obtained using responsivity ρ and OCPs in [7].

symbols.

$$\langle(\mathbf{p}_i - \mathbf{p}_j) \cdot \boldsymbol{\rho}\rangle \neq 0. \tag{11}$$

The region of CSK-1PD constellation points in terms of normalized electrical current is limited to one dimension (1-D) only as seen in Fig. 3. The 1-D region range depends on the responsivity of respective red, green and blue lights on the photodetector, as shown in (12). The maximum and minimum range of a constellation point (in terms of normalized electrical current) remains the same in an RGB LED as the highest, and lowest responsivity corresponds to red, and blue colour LEDs, respectively. Therefore, the values of all possible constellation points lie between the normalized electrical currents defined by the highest and lowest responsivities. The electrical symbols corresponding to the two extremes of responsivity values provides the maximum Euclidean distance between any two symbols in the constellation set. Hence, the additional range constraint, as shown in (13) has been included in the optimization process for complete range constraint. Constraint in (13) can be further reduced to (14), when the matrix $\mathbf{X0}$ and $\mathbf{X}$ have rows always arranged in increasing current fashion from top to bottom as seen in Table 1. The matrix arrangement has been kept the same in all the simulations and results. The constraints have been expressed as a set of linear equalities and inequalities as per *fmincon* solver.

$$\langle\,[0\,0\,1]\cdot\boldsymbol{\rho}\,\rangle \leq \langle\,\mathbf{p}_i\cdot\boldsymbol{\rho}\,\rangle \leq \langle\,[1\,0\,0]\cdot\boldsymbol{\rho}\,\rangle. \tag{12}$$

$$\max\{\langle\,(\mathbf{p}_i-\mathbf{p}_j)\cdot\boldsymbol{\rho}\,\rangle\} \leq |\langle\,[1\,0\,0]\cdot\boldsymbol{\rho}\,\rangle - \langle\,[0\,0\,1]\cdot\boldsymbol{\rho}\,\rangle|, \tag{13}$$

$$\langle\,(\mathbf{X0}_{R_4}-\mathbf{X0}_{R_1})\cdot\boldsymbol{\rho}\,\rangle \leq |\langle\,[1\,0\,0]\cdot\boldsymbol{\rho}\,\rangle - \langle\,[0\,0\,1]\cdot\boldsymbol{\rho}\,\rangle|. \tag{14}$$

The vector dot product changes to matrix dot product on considering all the four constellation points in a matrix, i.e., $\mathbf{X0}$. $\mathbf{X0}_{R_1}$, and $\mathbf{X0}_{R_4}$ represent the first, and fourth row of the matrix $\mathbf{X0}$. The results are simulated in matrix notation to obtain all four symbols in one go in the matrix notation $\mathbf{X}_o$.

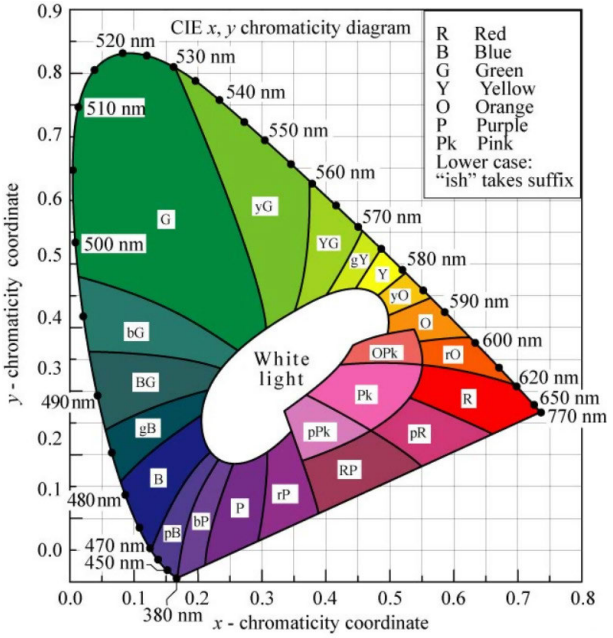

FIGURE 4. 1931 CIE chromaticity diagram with areas attributed to different colours [25].

C. MINIMUM EUCLIDEAN DISTANCE CONSTRAINT

The optimization process takes random initial constellation points, as shown in Table 1. The minimum Euclidean distance between any two symbols among all the symbols in the initial random constellation points, $\mathbf{X0}$, is taken as a constraint for next optimization iteration (t). The minimum Euclidean distance (MED) constraint is updated according to the successive optimized constellation points ($\mathbf{X}$) in $(t+1)$ iteration of β for much faster convergence. The only difference in this constraint for uniform (in (15)) and non-uniform (in (16)) input data is the logarithmic factor.

$$d_k(t+1) \geq min\,\{d_k(t)\}, \tag{15}$$

$$d_k(t+1) \geq min\,\{d_k(t)\ln\frac{p(s_j)}{p(s_i)}\},\quad s.t.\ p(s_i) \geq p(s_j). \tag{16}$$

D. STRICT WHITE TONE CONSTRAINT

CSK systems practically should have a white tone operating color. IEEE 802.15.7 standard for VLC accepts the most widely used model of human color perception, CIE 1931, to adhere to all applicable luminary standards. The CIE 1931 chromaticity gamut [25] has been shown in Fig. 4. The color of any visible light wavelength can be represented by the chromaticity coordinates (x, y). CIE 1931 color space typically considers eleven mean white tonalities at different color temperatures for white light evaluation. Table 2, shows the chromaticity coordinates producing white tones.

The constellation points consist of RGB LED optical power vector for a given symbol. The (x, y) chromaticity coordinates have been represented by (x, y) coordinates in the rest of the paper. Equation (17) provides a relation between

TABLE 2. Mean white tonalities having different temperatures in CIE 1931 RGB colour space.

Serial No.	Coordinates		White Color Temperature, T_c(K)
	x	y	
1	0.418	0.390	3100
2	0.389	0.362	3500
3	0.369	0.350	4000
4	0.354	0.340	4500
5	0.342	0.333	5000
6	0.334	0.328	5500
7	0.324	0.321	6000
8	0.317	0.317	6500
9	0.310	0.313	7000
10	0.305	0.310	7500
11	0.300	0.305	8000

x, y chromaticity coordinates and LED output power for a given wavelength of light. Hence, from **X0** one can find the value of (x, y) in the CIE 1931 chromaticity diagram as follows

$$\begin{aligned} x &= x_r P_r + x_g P_g + x_b P_b, \\ y &= y_r P_r + y_g P_g + y_b P_b, \end{aligned} \tag{17}$$

where the coordinates of central wavelength of red LED light is (x_r, y_r), green LED light is (x_g, y_g) and blue LED light is (x_b, y_b) in the CIE chromaticity color space. The central wavelength coordinates are known from the CIE 1931 color space as shown in Table 3. The CSK-1PD constellation symbols on an average should emit white colour light. The average white tone can be obtained in terms of chromaticity coordinates as

$$(\overline{x}, \overline{y}) = \sum_{i}^{M} p(s_i)(x, y)_{s_i}, \tag{18}$$

where $p(s_i)$ is the probability of symbol s_i, and $(\overline{x}, \overline{y})$ are the chromaticity coordinates representing the average perceived color of the transmitted symbols. When $(\overline{x}, \overline{y})$ represents a perceived white color from any of the eleven mean white tones (refer Table 2), the constellation symbols are said to have a white color balance. In order to fix the perceived color to white tone, an average white tone constraint is required on the constellation symbols as follows

$$(\overline{x}, \overline{y}) \in \{(0.418, 0.390), \ldots, (0.300, 0.305)\}, \tag{19}$$

$\{(0.418, 0.390), \ldots, (0.300, 0.305)\}$ forms the set of eleven mean white tones. The optimization is done by considering one out of eleven mean white tones at a time which makes it a strict constraint. The average white tone constraint is given by the affine equality for a color temperature of 3100 K, $(\overline{x}, \overline{y}) = (0.418, 0.390)$. Similarly, optimization is done for all other white tones.

The average tone of optimized constellation points without color constraint obtained and shown in the results section for different source distributions has been calculated to know the chromaticity coordinates. It is clear from Table 4, that none of them fulfills the white tone balance. Therefore, a white tone constraint is required for maintaining an average white tone in the constellation points. There is a limitation to this white tone constraint as the OCPs with strict white tone constraint reduces the SNR gain of the system in comparison to the OCPs without white tone constraint. Further, not all the white tones can be achieved by the constellation points optimized for minimum SNR. However, the desired white tones are achieved with reduced SNR performance. Therefore, the authors have explored two alternatives to manage white tones in the optimized CSK constellation points.

TABLE 3. The corresponding coordinates of central wavelengths of RGB LEDs in CIE 1931 color space.

LED light color	Wavelength	Coordinates	
		x	y
Red	640 nm	0.7190	0.2809
Green	530 nm	0.1547	0.8059
Blue	465 nm	0.1355	0.0399

TABLE 4. The average tone coordinates of different source distributions.

Source Distribution	Coordinates	
	$\overline{x}$	$\overline{y}$
Uniform	0.3877	0.2541
Maxwell-Boltzmann	0.2152	0.1567
Exponential	0.2216	0.1439
Pareto	0.2146	0.1413

IV. SOLUTIONS FOR AVERAGE WHITE LIGHT

The CIE 1931 chromaticity diagram in Fig. 4 shows a wide area for white light. The strict white tone constraint can be extended to the whole white region to achieve SNR gain close to OCPs of without white tone constraint. The white region constraint has been derived in section IV-A, which relaxes the strictness of the previous mean white tone constraint. Another way to obtain white tone output light can be the addition of another RGB LED at the transmitter side. The use of an extra RGB LED helps in maintaining white tone without even disturbing the OCPs obtained without considering the white tone constraint. The extra RGB LED method has been described in section IV-B.

A. RELAXED WHITE TONE CONSTRAINT

The strict white tone constraint considers only eleven mean white tones, so it is not possible to get optimized constellation points for all the eleven white tones. The relaxed white tone constraint regards any (x, y) coordinates falling inside the white region (see Fig. 4) as desired white. The white light region has been extracted out from the CIE 1931 chromaticity diagram in Fig. 5 for deriving the approximate mathematical model of the region. Every (x, y) coordinates in the whole white region does not give pure white light; however, (x, y) coordinates inside the white light region has been considered in designing LEDs in literature [26]–[29]. There is a trade-off between the purity of white tone and SNR performance; the focus of the proposed work is to obtain optimized constellation points which maintain the bare minimum acceptable white light.

The desired (x, y) coordinates of the OCPs lie inside the white light region, which is an irregular shape. The research

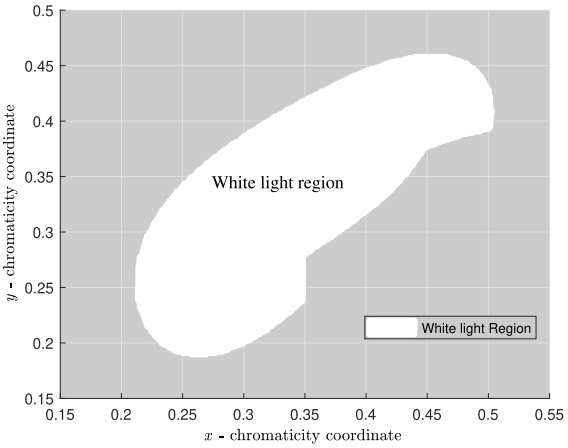

FIGURE 5. White light region extracted from the 1931 CIE chromaticity diagram.

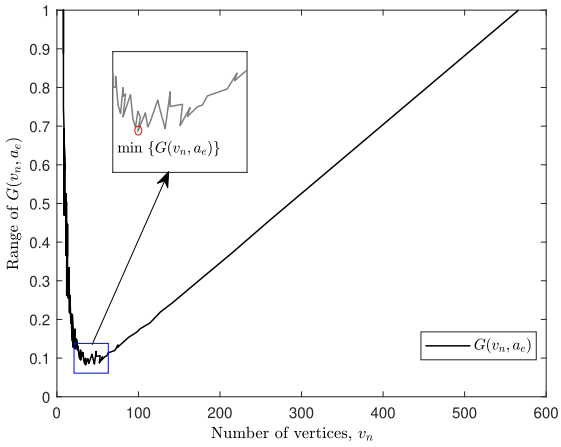

FIGURE 6. The minimum value obtained for $G(v_n, a_e)$.

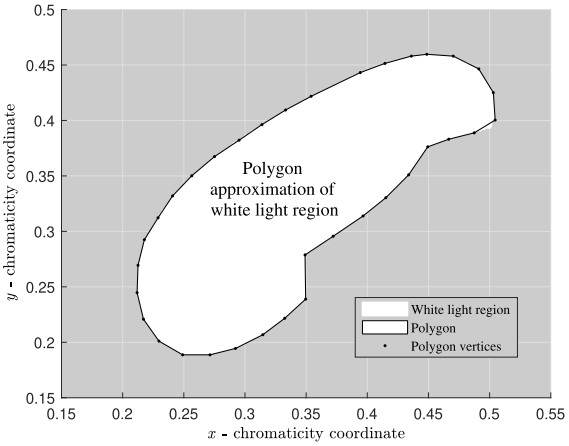

FIGURE 7. Polygon approximation of the white light region.

literature is replete with algorithms to determine whether a point is within a polygon or not. Therefore, the most common approach is to first approximate an irregular shape into a polygon from the set of points, R forming the irregular shape. Once the irregular shape is decomposed to a polygon, deciding whether a point lies inside is the point-in-polygon (PIP) test problem. The irregular shape can be decomposed to triangles using polygon triangulation method [30]. The triangulation method chooses a subset of points, P from the set R to approximate the white region as a mesh of triangles. All the P points form the vertices of the white light region, hence with the triangulation method, the white region can be approximated to an arbitrary polygon with few points. In polygonal representation, the curved shapes are represented using tangential approximations in the form of straight lines, which ultimately depends on the number of vertices considered. Therefore, there is always an approximation error (a_e), which can be realized in terms of percentage of area left uncovered by the polygon approximation. Since the white region is in two dimensions (2-D) only, there are a number of algorithms for the 2-D PIP problem. The authors opted for the efficient standard algorithm in paper [31], which is capable of solving PIP problem for any arbitrary polygon, convex or non-convex. Further, during the optimization process, the algorithm shall be called so often, hence an accelerated algorithm that grows linearly with the number of polygon vertices, v_n, is a viable choice. Therefore, the complexity of the PIP algorithm used in this work is $O(v_n)$. The polygonal representation of white light region depends on PIP algorithm as well and thus becomes an optimization problem as follows:

$$\begin{aligned} v_n &= \min \ \{G(v_n, a_e)\}, \\ \text{where, } G(v_n, a_e) &= O(v_n) + a_e, \end{aligned} \tag{20}$$

where a_e decreases with more number of v_n while the PIP algorithm complexity increases with more number of v_n. The complexity and approximation error values have been normalized to [01]. They have been weighted equally in the minimization problem. The number of vertices which provides minimum complexity and area error has been obtained and shown in Fig. 6. The white light region ($\mathcal{W}$) in the CIE 1931 chromaticity diagram has been approximated to a polygon in Fig. 7 with vertices, $v_n = 35$.

The relaxed white tone constraint ensures $(\overline{x}, \overline{y}) \in \mathcal{W}$, and has been formulated as follows:

$$PIP_{alg}(\overline{x}, \overline{y}, x_P, y_P) - 1 = 0, \tag{21}$$

where, x_P and y_P belongs to the x and y coordinates of polygon points P. The PIP algorithm returns logical 1, whenever a point is inside or on the polygon.

B. EXTRA RGB LED

Researchers have used scrambler for maintaining white tone in CSK-1PD [7]. Linear feedback shift register (LFSR) based scrambler is not very expensive; however, its complexity increases with increase in the length, l. The color balance in [7] is achieved for uniform input data at $l > 20$. The input data scrambled for length $l > 20$, provides color balance by averaging (P_r, P_g, P_b) to get values around (0.33, 0.33, 0.33), which corresponds to a single chromaticity coordinates (0.3330, 3718). The scrambler needs to be designed

specifically for different PS input data, and a particularly designed scrambler can produce only one type of white tone. The scramblers used for this purpose are usually additive, so it must be reset by the frame synchronization bits otherwise massive error propagation happens [4]. Further, with the non-uniformity in the input data, the length in scrambler may increase, which in turn increases the complexity drastically.

In order to escape the problems mentioned above, the authors in this article have suggested the utilization of an extra RGB LED at the transmitter to maintain any white tone in the white light region without hampering the SNR gain obtained from specific OCPs for source distributions. One can design a constant color light with the extra RGB LED to mix with the RGB modulated symbols to produce the desired average white tone $(\bar{x}_d, \bar{y}_d)$. It provides flexibility and removes the constraint on the length or number of the input symbols. Further, RGB LEDs being inexpensive does not incur much cost to the system. The chromaticity coordinates (x_e, y_e) of extra RGB LED can be obtained as

$$x_e = \frac{(\bar{x}_d(Y_1 + Y_e) - \bar{x})}{Y_e},$$
$$y_e = \frac{(\bar{y}_d(Y_1 + Y_e) - \bar{y})}{Y_e}, \tag{22}$$

where Y_e and Y_1 are the luminance corresponding to extra RGB LED chromaticity coordinates, and average tone coordinates obtained from the specific OCPs for source distributions, respectively. The normalized range of luminance is between 0 to 1 [32]. (x_e, y_e) can be expressed in the form of RGB LEDs optical powers by substituting (17) in (22) with the following constraint

$$P_r + P_g + P_b = 1,$$
$$\text{where, } (P_r, P_g, P_b) \geq 0 \text{ and } 1 \geq Y_e > 0. \tag{23}$$

The computational complexity of this method depends on designing the RGB optical powers of extra LED, which forms linear equations in five variables on considering (22) and (23). There are five unknown variables with their respective upper and lower bounds and three linear equations. Therefore the linear equations are solved for different values of Y_1 to obtain (Pr, Pg, Pb) in terms of Y_e and then Y_e can be obtained from (23). The PD receives the combined light of RGB modulated and extra RGB LED signal. The receiver side knows the excess current generated because of the additional RGB LED. The total current generated shifts the symbols with additional electric current values, hence on subtracting the incremental current yields corresponding current of the modulated signal. It is analogous to removing the constant ambient light noise at the VLC receiver. Henceforth, with linear computational complexity at the transmitter and receiver, the concept of using an extra RGB LED can be a better option for colour rendering and balancing.

V. RESULTS AND DISCUSSION

The SNR performance gain with respect to SER for 4-CSK-1PD with and without white tone for uniform and non-uniform input data has been obtained and reasoned in the following sections. The simulation parameters have been kept same for this work as in [19] for fair comparison. The list of simulation parameters have been shown in Table. 5. The possibility of maintaining any desired white tone has been validated by finding non-negative RGB optical powers for the desired white tone in section V-C.

TABLE 5. Simulation parameters for CSK-1PD.

Parameters	Value
Distance between Transmitter and Receiver	100 cm
Number of LEDs	1 (RGB)
RGB Optical power	1 mW
Photodetector responsivity	[0.42, 0.32, 0.22]
Mode number	45
Photodetector area	92 mm^2

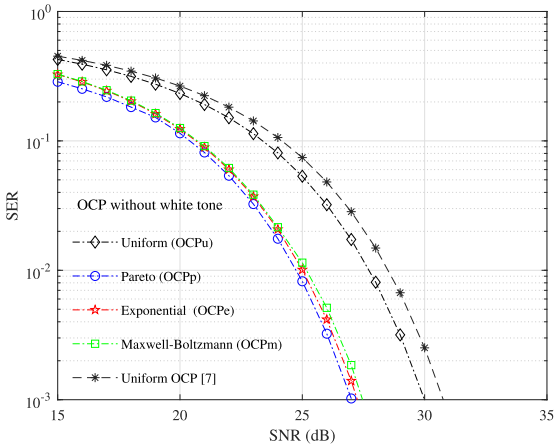

FIGURE 8. SER versus SNR plot of different source distribution at their specific optimized constellation points.

A. WITHOUT WHITE TONE CONSTRAINT

Table. 6 shows the OCPs of all the source distributions considering all constraints as discussed in section III except white tone constraint. The SNR in dB for FEC limit SER can be observed in Fig. 8 for different source distributions utilizing their specific OCPs.

It has been observed that the optimized constellation points for uniform input data (OCPu) perform better than the OCP of uniform source distribution from [7] by 0.75 dB. The OCPu results in equidistant normalized electric current symbols, which is equivalent to the analytically known global optimum placement of equiprobable symbols in pulse amplitude modulation (PAM) for minimum SER [20]. The normalized design range for CSK-1PD is just a straight line, so following the equidistant symbol spacing criteria for equiprobable symbols yields the same $d_i = 0.0667$ for all i (check equation (8) for d_i). The OCPu achieve a minimum Euclidean distance of 0.0667 for all d_i.

It has been observed that the SNR performance of non-uniform source distributions utilizing specific OCPs

TABLE 6. Optimized CSK-1PD constellation points for uniform, exponential, Maxwell-Boltzmann, and Pareto input data without white tone constraint.

Distributions:	Uniform			Exponential			Maxwell-Boltzmann			Pareto		
RGB powers:	P_r	P_g	P_b	P_r	P_g	P_b	P_r	P_g	P_b	P_r	P_g	P_b
$\mathbf{p}_1$	0	0	1	0	0	1	0	0	1	0	0	1
$\mathbf{p}_2$	0.1880	0.2905	0.5215	0.2261	0.2803	0.4936	0.2084	0.3096	0.482	0.2185	0.3109	0.4706
$\mathbf{p}_3$	0.5217	0.2902	0.1881	0.5939	0.2252	0.1809	0.5531	0.2793	0.1676	0.5606	0.2768	0.1626
$\mathbf{p}_4$	1	0	0	1	0	0	1	0	0	1	0	0

TABLE 7. SNR of CSK-1PD without considering the white tone constraint for different source distributions with specific OCPs and uniform OCPs [7] for all distributions.

Input data distribution type	SNR (dB) at SER of 10^{-3} considering OCP without white tone constraint:	
	uniform OCP [7]	Specific OCP(u,m,e,p)
Uniform	30.75	30
Maxwell-Boltzmann	29.50	27.4
Exponential	29.00	27.25
Pareto	28.05	27

TABLE 8. Optimized CSK-1PD constellation points with strict white tone constraint for uniform and Pareto input data.

Source Distribution	P_r	P_g	P_b	Mean white tone coordinates $(\overline{x}, \overline{y})$
Uniform	0	0.056	0.944	(0.334, 0.328) at temperature 5500K
	0.1	0.35	0.55	
	0.255	0.65	0.095	
	0.969	0.031	0	
Pareto	0	0	1	(0.369, 0.350) at temperature 4000K
	0.11	0.343	0.547	
	0.52	0.38	0.1	
	1	0	0	

obtained in this work provides improved SNR gain as compared to the work in [19], where OCPs designed in [7] for uniform source distribution was utilized. The respective SNR values have been tabulated for comparison in Table 7. In the case of specific OCPs, the constellations points are further optimized by geometrically shaping the symbols based on their probability of occurrence. Therefore, the improved performance of non-uniform distributions in case of specific OCPs is because of the consecutive PS based GS technique. It is interesting to note that with specific OCPs the performance of non-uniform source distributions approach close to each other which is again due to the specific shifting of symbols according to PS.

B. WITH WHITE TONE CONSTRAINT

The constellation points are optimized so as to get average white tone light as the transmitted output.

1) STRICT CONSTRAINT

The constellation points are obtained considering all constraints in section III along with strict white tone constraint in (19). The OCPs obtained with strict white tone are abbreviated as S-OCPs. The uniform and Pareto (non-uniform) source distribution OCPs are obtained and shown in Table. 8.

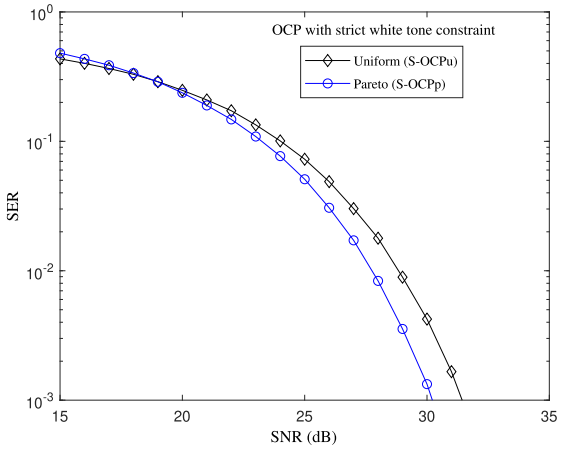

FIGURE 9. SER versus SNR plot of uniform and Pareto source distributions with optimized constellation points maintaining mean white tones as shown in Table. 8.

The corresponding mean white tone chromaticity coordinates can be seen in the last column. The SER versus SNR plots in Fig. 9, demonstrates the impediment of considering strict white tone constraint. The SNR for uniform distribution is 31.4 dB and for Pareto is 30.2 dB at 10^{-3} SER. It can be observed that the performance of both uniform and Pareto have decreased from OCPu and OCPp, respectively. The chromaticity coordinates of the four OCPs do not lie in the white region except one, and for maintaining average white tone, the optimum position of symbols in terms of SNR is changed and therefore reduces the SNR gain.

2) RELAXED CONSTRAINT

In this case, the whole white region has been considered in the white tone constraint of the optimization process. Table. 9 shows the OCPs of all the source distributions considering all constraints and the relaxed white tone constraint. The respective white tone coordinates can be seen at the last row. The SNR at FEC limit SER can be observed in Fig. 10 for different source distributions considering OCPs for relaxed white tone (R-OCPs). The SNR values for FEC limit SER have been enumerated in Table. 10 for comparison. It has been observed that SNR performance gain of uniform has achieved the optimum SNR gain of OCPu. The equiprobability of symbols in uniform distribution assist it to render ideal white color balance with optimum SNR gain. However, for non-uniform distributions, SNR gain has improved from the strict white tone constraint, whereas it is still less than the without white tone OCPs performance gain. The range

TABLE 9. Optimized CSK-1PD constellation points with relaxed white tone constraint for uniform, exponential, Maxwell-Boltzmann, and Pareto distributed input data.

Distributions:	Uniform			Exponential			Maxwell-Boltzmann			Pareto		
RGB powers:	P_r	P_g	P_b	P_r	P_g	P_b	P_r	P_g	P_b	P_r	P_g	P_b
$\mathbf{p}_1$	0	0	1	0.0234	0.0782	0.8984	0.0202	0.0625	0.9172	0.0262	0.0954	0.8784
$\mathbf{p}_2$	0.1507	0.3655	0.4837	0.1795	0.4144	0.4061	0.2069	0.4096	0.3835	0.1916	0.4218	0.3866
$\mathbf{p}_3$	0.4842	0.3653	0.1505	0.5842	0.2847	0.1312	0.5743	0.3011	0.1245	0.5930	0.2790	0.1277
$\mathbf{p}_4$	1	0	0	1	0	0	1	0	0	1	0	0
Average White tone: coordinates $(\overline{x}, \overline{y})$	(0.3504, 0.3424)			(0.2247, 0.2115)			(0.2247, 0.2115)			(0.2247, 0.2114)		

TABLE 10. SNR of CSK-1PD at specific OCPs for different source distributions with and without white tone constraint.

Input data distribution type	SNR (dB) at SER of 10^{-3} considering OCP without and with white tone constraint:	
	OCP(u,m,e,p)	R-OCP(u,m,e,p)
Uniform	30	30
Maxwell-Boltzmann	27.4	28.65
Exponential	27.25	28.7
Pareto	27	28.44

TABLE 11. Optical powers of extra RGB LED for the desired white tone of CSK-1PD at specific OCPs of Pareto source distribution.

No.	Desired white-tone coordinates		Average tone luminance	Extra LED RGB powers			Extra LED chromaticity coordinates and luminance		
	x_d	y_d	Y_1	P_r	P_g	P_b	x_e	y_e	Y_e
1.	0.3496	0.2389	0.01	0.3644	0.1465	0.4891	0.3509	0.2399	1
2.	0.2751	0.3674	0.01	0.2285	0.3586	0.4129	0.2757	0.3697	1
3.	0.3496	0.2389	0.1	0.3851	0.1514	0.4635	0.3631	0.2487	1
4.	0.2751	0.3674	0.1	0.2371	0.3825	0.3804	0.2812	0.3900	1
5.	0.3496	0.2389	1	0.5917	0.2011	0.2072	0.4846	0.3365	1
6.	0.2751	0.3674	1	0.3226	0.6212	0.0562	0.3357	0.5935	1

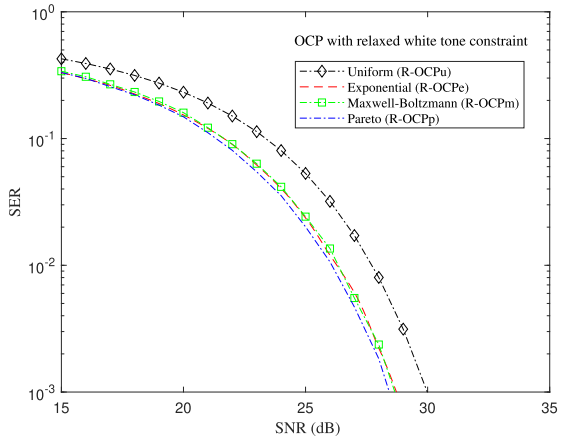

FIGURE 10. SER versus SNR plot of different source distributions using optimized constellation points with relaxed white tone constraint.

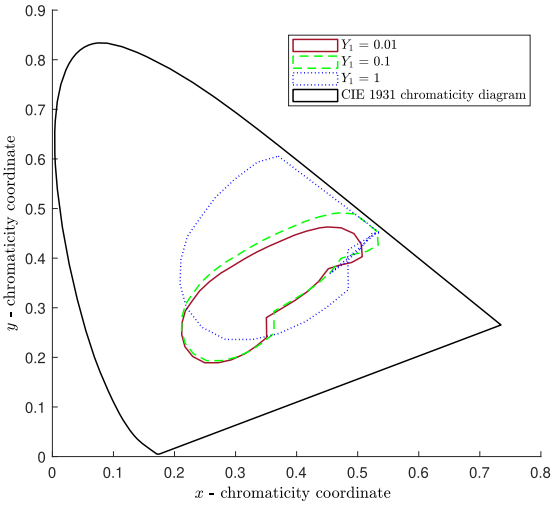

FIGURE 11. Extra RGB LED coordinates for Pareto source distribution forming polygon for the white light region.

of choice of chromaticity coordinates has increased here tremendously, and hence the performance of the R-OCPs in comparison to S-OCPs. The non-uniformity of symbols with s_1 ($\mathbf{p}_1$ in terms of RGB power) as highest probable symbol sabotage the reach to optimum SNR gain in R-OCPs. Moreover, the average white tone chromaticity coordinates of non-uniform source distributions are precisely the same, but the OCPs are different. The reason behind this comes from Table. 4, where the average tone of non-uniform distributions is close to each other. Hence, during optimization with white tone constraint, the different distributions look for a nearby valid white tone coordinates for optimized SNR gain with distinct OCPs.

C. WITH EXTRA RGB LED

The chromaticity coordinates of extra RGB LED for the vertices of the white light region (see Fig. 7) in Pareto distribution have been obtained and shown in Fig. 11 for different values of luminance Y_1. The extra RGB LED coordinates gets skewed to remain inside the CIE chromaticity diagram. The non-negative RGB optical powers of LED fulfilling all

the linear equalities and inequalities have been obtained. The RGB optical powers obtained for the extra LED can be viewed in Table. 11.

VI. CONCLUSION

This article, for the very first time, tries to optimize the constellation points of CSK-1PD with and without average white tone for uniform and non-uniform (exponential, Maxwell-Boltzmann, and Pareto) source distributions. The specific OCPs without white tone constraint gives improved SNR performance gain in all the source distributions with respect to the OCPs of [7]. However, the OCPs with strict white tone constraint maintains the white tone on an average with SNR gain reduced by 1.4 dB and 3.2 dB from without white tone constraint for uniform and Pareto distribution, respectively. The optimization process for OCPs with relaxed white tone constraint considers the whole white region in white tone constraint to boost the SNR gain. The R-OCPs for uniform input data achieves the same SNR gain (30 dB) as OCPu. However, for non-uniform, the R-OCPs still performs 1.25-1.45 dB lesser than the non-uniform OCPs without white tone constraint. Furthermore, this article proposes a novel solution to use two RGB LEDs at the transmitter, one for modulation and another for maintaining white tone. It has been observed from results that the RGB optical powers of extra RGB LED can be designed for any desired chromaticity coordinates inside the white light region retaining maximum SNR gain with specific OCPs for uniform and non-uniform source distributions.

ACKNOWLEDGMENT

This publication is an outcome of the Research and Development work undertaken project under the Visvesvaraya Ph.D. Scheme of Ministry of Electronics and Information Technology, Government of India, being implemented by Digital India Corporation.

REFERENCES

[1] N. Chi, H. Haas, M. Kavehrad, T. D. C. Little, and X.-L. Huang, "Visible light communications: Demand factors, benefits and opportunities [guest editorial]," *IEEE Wireless Commun.*, vol. 22, no. 2, pp. 5–7, Apr. 2015.

[2] L. E. M. Matheus, A. Borges Vieira, L. F. M. Vieira, M. A. M. Vieira, and O. Gnawali, "Visible light communication: Concepts, applications and challenges," *IEEE Commun. Surveys Tuts.*, vol. 21, no. 4, pp. 3204–3237, 4th Quart., 2019.

[3] R. Ahmad and A. Srivastava, "PAPR reduction of OFDM signal through DFT precoding and GMSK pulse shaping in indoor VLC," *IEEE Access*, vol. 8, pp. 122092–122103, 2020.

[4] *IEEE Standard for Local and Metropolitan Area Networks—Part 15.7: Short-Range Optical Wireless Communications*, Standard 802.15.7-2018 (Revision of IEEE Std 802.15.7-2011), Apr. 2019, pp. 1–407.

[5] E. Monteiro and S. Hranilovic, "Design and implementation of color-shift keying for visible light communications," *J. Lightw. Technol.*, vol. 32, no. 10, pp. 2053–2060, May 2014.

[6] A. Wilkins, J. Veitch, and B. Lehman, "LED lighting flicker and potential health concerns: IEEE standard PAR1789 update," in *Proc. IEEE Energy Convers. Congr. Expo.*, Sep. 2010, pp. 171–178.

[7] J. M. Luna-Rivera, V. Guerra, J. Rufo-Torres, R. Perez-Jimenez, C. Suarez-Rodriguez, and J. Rabadan-Borges, "Low-complexity colour-shift keying-based visible light communications system," *IET Optoelectron.*, vol. 9, no. 5, pp. 191–198, Oct. 2015.

[8] Thorlabs. (2020). *PDA36A2 Si Switchable Gain Detector User Guide*. Accessed: Jun. 30, 2020. [Online]. Available: https://www.thorlabs.com/drawings/989677a28de218d7-D5E11041-F2E3-267D-2BA75E2F8CF8666B/PDA36A2-Manual.pdf

[9] A. Burton, H. Le Minh, Z. Ghassemlooy, S. Rajbhandari, and P. A. Haigh, "Performance analysis for 180o receiver in visible light communications," in *Proc. 4th Int. Conf. Commun. Electron. (ICCE)*, Aug. 2012, pp. 48–53.

[10] D. N. Anwar and A. Srivastava, "VLC-based safe, low-cost, and accurate healthcare system for video EEG using colour constellation scheme," *Proc. SPIE*, vol. 10685, May 2018, Art. no. 1068549.

[11] D. U. Campos-Delgado, J. M. Luna-Rivera, R. Perez-Jimenez, C. A. Gutierrez, V. Guerra, and J. Rabadan, "Constellation design for color space-based modulation in visible light communications," *Phys. Commun.*, vol. 31, pp. 154–159, Dec. 2018.

[12] R. J. Drost and B. M. Sadler, "Constellation design for color-shift keying using billiards algorithms," in *Proc. IEEE Globecom Workshops*, Dec. 2010, pp. 980–984.

[13] R. J. Drost and B. M. Sadler, "Constellation design for channel precompensation in multi-wavelength visible light communications," *IEEE Trans. Commun.*, vol. 62, no. 6, pp. 1995–2005, Jun. 2014.

[14] E. Monteiro and S. Hranilovic, "Constellation design for color-shift keying using interior point methods," in *Proc. IEEE Globecom Workshops*, Dec. 2012, pp. 1224–1228.

[15] Q. Gao, R. Wang, Z. Xu, and Y. Hua, "Power-efficient high-dimensional constellation design for visible light communications," in *Proc. Opto-Electron. Commun. Conf. (OECC)*, Jun. 2015, pp. 1–3.

[16] R. Chen, "Solution of minimax problems using equivalent differentiable functions," *Comput. Math. Appl.*, vol. 11, no. 12, pp. 1165–1169, Dec. 1985.

[17] X. Han and I. B. Djordjevic, "Probabilistically shaped 8-PAM suitable for data centers communication," in *Proc. 20th Int. Conf. Transparent Opt. Netw. (ICTON)*, Jul. 2018, pp. 1–4.

[18] Z. Qu and I. B. Djordjevic, "On the probabilistic shaping and geometric shaping in optical communication systems," *IEEE Access*, vol. 7, pp. 21454–21464, 2019.

[19] D. N. Anwar and A. Srivastava, "Design and analysis of probabilistic shaping in color shift keying modulation schemes," *IEEE Syst. J.*, early access, Jul. 21, 2020, doi: 10.1109/JSYST.2020.3007391.

[20] K. Vasudevan, *Digital Communications and Signal Processing*, 2nd ed. Chennai, India: Univ. Press (India) Pvt. Ltd., 2010.

[21] Z. Qu, I. B. Djordjevic, and J. Anderson, "Two-dimensional constellation shaping in fiber-optic communications," *Appl. Sci.*, vol. 9, no. 9, p. 1889, May 2019.

[22] J. Nocedal and S. J. Wright, *Numerical Optimization*. New York, NY, USA: Springer-Verlag, 1999.

[23] P. Charbonnea, "An introduction to genetic algorithms for numerical optimization," National Center for Atmospheric Research, Boulder, CO, USA, Tech. Note NCAR/TN-450+IA, Mar. 2002. [Online]. Available: http://cobweb.cs.uga.edu/~potter/CompIntell/no_tutorial.pdf

[24] B. Moore, G. Takahara, and F. Alajaji, "Pairwise optimization of modulation constellations for non-uniform sources," *Can. J. Electr. Comput. Eng.*, vol. 34, no. 4, pp. 167–177, 2009.

[25] E. F. Schubert, *Light Emitting Diodes*, 2nd ed. Cambridge, U.K.: Cambridge Univ. Press, 2006.

[26] W. Young Kim, Y.-H. Kim, C.-G. Jhun, R. Wood, P. Mascher, and C.-B. Moon, "Spectroscopic study of white organic light-emitting devices with various thicknesses of emissive layer," *J. Appl. Phys.*, vol. 111, no. 1, Jan. 2012, Art. no. 014507.

[27] K. L. Kosanke and B. J. Kosanke, "Selected pyrotechnic publications of KL and BJ kosanke—Part 1: 1981 through 1989," in *Pyrotechnic Literature Series*. Whitewater, CO, USA: Journal of Pyrotechnics, Inc., 1995.

[28] V. Singh and A. K. Mishra, "White light emission from vegetable extracts," *Sci. Rep.*, vol. 5, no. 1, p. 11118, Jun. 2015.

[29] P. Babu, K. H. Jang, E. S. Kim, L. Shi, and H. J. Seo, "Optical properties and white-light emission in Dy3+-doped transparent oxyfluoride glass and glass ceramics containing CaF_2 nanocrystals," *J. Korean Phys. Soc.*, vol. 54, no. 4, pp. 1488–1491, Apr. 2009.

[30] A. Narkhede and D. Manocha, "Fast polygon triangulation based on seidel's algorithm," in *Graphics Gems V*, New York, NY, USA: Academic, 1995, ch. VII.5, pp. 394–397.

[31] K. Hormann and A. Agathos, "The point in polygon problem for arbitrary polygons," *Comput. Geometry*, vol. 20, no. 3, pp. 131–144, Nov. 2001.

[32] M. W. Hodapp, "Applications for high-brightness light-emitting diodes," in *Semiconductors and Semimetals*. New York, NY, USA: Academic, 1997, ch. 6, pp. 227–356.

DIL NASHIN ANWAR (Graduate Student Member, IEEE) received the B.Tech. and M.Tech. degrees from the Department of Electronics and Communication Engineering, Aligarh Muslim University (AMU), Aligarh, in 2013 and 2015, respectively. She is currently pursuing the Ph.D. degree with the Department of Electronics and Communication Engineering, IIIT-Delhi. As a Research Assistant, she has worked in the classification of EEG signals with IIIT-Delhi, till 2017. She is also a Visvesvaraya Ph.D. Fellow, supported by DeitY, Government of India. Her research interests include visible light communication and light fidelity (Li-Fi) in the Internet of Things (IoT).

ANAND SRIVASTAVA (Member, IEEE) received the M.Tech. and Ph.D. degrees from IIT Delhi, India, in 2002. He has worked at Alcatel-Lucent-Bell Labs, India, from 2009 to 2012, and the Center for Development of Telematics (CDOT), a Telecom Research Center of the Government of India, from 1989 to 2008. He was the Dean and a Professor with the School of Computing and Electrical Engineering, IIT Mandi, India, from 2012 to 2014. He has been an Adjunct Faculty with IIT Delhi, since 2008. He has been the Dean and a Professor with IIIT-Delhi, since 2014. He was also closely involved with ITU-T, Geneva, in Study Group 15, and represented India for various optical networking standards meetings. His current research interests include optical core and access networks, fiber-wireless (FiWi) architectures, visible light communications (VLC), optical signal processing, and multi-band elastic optical networks (EON).